## CANCER IMMUNOTHERAPY

# Gut microbiome modulates response to anti–PD-1 immunotherapy in melanoma patients

V. Gopalakrishnan,[1,2]* C. N. Spencer,[2,3]* L. Nezi,[3]* A. Reuben,[1] M. C. Andrews,[1] T. V. Karpinets,[3] P. A. Prieto,[1]† D. Vicente,[1] K. Hoffman,[4] S. C. Wei,[5] A. P. Cogdill,[1,5] L. Zhao,[3] C. W. Hudgens,[6] D. S. Hutchinson,[7] T. Manzo,[3] M. Petaccia de Macedo,[6]‡ T. Cotechini,[8] T. Kumar,[3] W. S. Chen,[9] S. M. Reddy,[10] R. Szczepaniak Sloane,[1] J. Galloway-Pena,[11] H. Jiang,[1] P. L. Chen,[9]§ E. J. Shpall,[12] K. Rezvani,[12] A. M. Alousi,[12] R. F. Chemaly,[11] S. Shelburne,[3,11] L. M. Vence,[5] P. C. Okhuysen,[11] V. B. Jensen,[13] A. G. Swennes,[7] F. McAllister,[14] E. Marcelo Riquelme Sanchez,[14] Y. Zhang,[14] E. Le Chatelier,[15] L. Zitvogel,[16] N. Pons,[15] J. L. Austin-Breneman,[1]|| L. E. Haydu,[1] E. M. Burton,[1] J. M. Gardner,[1] E. Sirmans,[17] J. Hu,[18] A. J. Lazar,[6,9] T. Tsujikawa,[8] A. Diab,[17] H. Tawbi,[17] I. C. Glitza,[17] W. J. Hwu,[17] S. P. Patel,[17] S. E. Woodman,[17] R. N. Amaria,[17] M. A. Davies,[17] J. E. Gershenwald,[1] P. Hwu,[17] J. E. Lee,[1] J. Zhang,[3] L. M. Coussens,[8] Z. A. Cooper,[1,3]¶ P. A. Futreal,[3] C. R. Daniel,[4,2] N. J. Ajami,[7] J. F. Petrosino,[7] M. T. Tetzlaff,[6,9] P. Sharma,[5,19] J. P. Allison,[5] R. R. Jenq,[3]# J. A. Wargo[1,3]#**

Preclinical mouse models suggest that the gut microbiome modulates tumor response to checkpoint blockade immunotherapy; however, this has not been well-characterized in human cancer patients. Here we examined the oral and gut microbiome of melanoma patients undergoing anti–programmed cell death 1 protein (PD-1) immunotherapy (n = 112). Significant differences were observed in the diversity and composition of the patient gut microbiome of responders versus nonresponders. Analysis of patient fecal microbiome samples (n = 43, 30 responders, 13 nonresponders) showed significantly higher alpha diversity (P < 0.01) and relative abundance of bacteria of the Ruminococcaceae family (P < 0.01) in responding patients. Metagenomic studies revealed functional differences in gut bacteria in responders, including enrichment of anabolic pathways. Immune profiling suggested enhanced systemic and antitumor immunity in responding patients with a favorable gut microbiome as well as in germ-free mice receiving fecal transplants from responding patients. Together, these data have important implications for the treatment of melanoma patients with immune checkpoint inhibitors.

Tremendous advances have been made in the treatment of melanoma and other cancers by using immune checkpoint inhibitors targeting the cytotoxic T lymphocyte–associated antigen 4 (CTLA-4) and programmed cell death protein 1 (PD-1); however, responses to these therapies are often heterogeneous and not durable (1–3). It has recently emerged that factors beyond tumor genomics influence cancer development and therapeutic responses (4–7), including host factors such as the gastrointestinal (gut) microbiome (8–10). A number of studies have shown that the gut microbiome may influence antitumor immune responses by means of innate and adaptive immunity (11, 12) and that therapeutic responses may be improved through its modulation (13, 14); however, this has not been extensively studied in cancer patients.

To better understand the role of the microbiome in response to immune checkpoint blockade, we prospectively collected microbiome samples from patients with metastatic melanoma starting treatment with anti–PD-1 therapy (n = 112 patients) (fig. S1 and table S1). Oral (buccal) and gut (fecal) microbiome samples were collected at treatment initiation, and tumor biopsies and blood samples were collected at matched pretreatment time points when possible, to assess for genomic alterations as well as the density and phenotype of tumor-infiltrating and circulating immune cell subsets (Fig. 1A and fig. S2). Taxonomic profiling using 16S ribosomal RNA (rRNA) gene sequencing was performed on all available oral and gut samples, with metagenomic whole-genome shotgun (WGS) sequencing performed on a subset (n = 25). Eligible patients (n = 89) were classified as responders (R, n = 54) or nonresponders (NR, n = 35) on the basis of radiographic assessment using the response evaluation criteria in solid tumors (RECIST 1.1) (15) at 6 months after treatment initiation. Patients were classified as R if they achieved an objective response (complete or partial response or stable disease lasting at least 6 months) or NR (progressive disease or stable disease lasting less than 6 months). This classification accounts for the subset of patients who may derive long-term disease benefit despite not achieving a bona fide RECIST response and has been used in numerous published studies of patients on checkpoint blockade (16–19). Of note, patients in R and NR groups were similar with respect to age, gender, primary type, prior therapy, concurrent systemic therapy, and serum lactate dehydrogenase (table S2). Prior genomic analyses have demonstrated that patients with tumors that have a higher mutational load are more likely to respond to anti–CTLA-4 (16, 20, 21) or anti–PD-1 therapy (21–24); however, a high mutational load alone appears neither sufficient nor essential for response. In this cohort, the total number of mutations and specific melanoma driver mutations were within comparable parameters between R and NR after anti–PD-1 therapy (fig. S3), though the number of tumors available for sequencing (n = 10, R = 7, NR = 3) was limited and may have reduced our ability to detect a significant association between mutational burden and response.

We first assessed the landscape of the oral and gut microbiome in all available samples in patients (n = 112) with metastatic melanoma using 16S

[1]Department of Surgical Oncology, The University of Texas MD Anderson Cancer Center, Houston, TX 77030, USA. [2]Department of Epidemiology, Human Genetics and Environmental Sciences, University of Texas School of Public Health, Houston, TX 77030, USA. [3]Department of Genomic Medicine, The University of Texas MD Anderson Cancer Center, Houston, TX 77030, USA. [4]Department of Epidemiology, The University of Texas MD Anderson Cancer Center, Houston, TX 77030, USA. [5]Department of Immunology, The University of Texas MD Anderson Cancer Center, Houston, TX 77030, USA. [6]Department of Translational Molecular Pathology, The University of Texas MD Anderson Cancer Center, Houston, TX 77030, USA. [7]Department of Molecular Virology and Microbiology, Baylor College of Medicine, Houston, TX 77030, USA. [8]Department of Cell, Developmental and Cell Biology, Oregon Health and Sciences University, Portland, OR 97239, USA. [9]Department of Pathology, The University of Texas MD Anderson Cancer Center, Houston, TX 77030, USA. [10]Department of Breast Medical Oncology, The University of Texas MD Anderson Cancer Center, Houston, TX 77030, USA. [11]Department of Infectious Diseases, The University of Texas MD Anderson Cancer Center, Houston, TX 77030, USA. [12]Department of Stem Cell Transplantation, The University of Texas MD Anderson Cancer Center, Houston, TX 77030, USA. [13]Department of Veterinary Medicine and Surgery, The University of Texas MD Anderson Cancer Center, Houston, TX 77030, USA. [14]Department of Clinical Cancer Prevention, The University of Texas MD Anderson Cancer Center, Houston, TX 77030, USA. [15]Centre de Recherche de Jouy-en-Josas, Institut National de la Recherche Agronomique, 78352 Jouy-en-Josas, France. [16]Centre d'Investigation Clinique Biothérapie, Institut Gustave-Roussy, 94805 Villejuif Cedex, France. [17]Department of Melanoma Medical Oncology, The University of Texas MD Anderson Cancer Center, Houston, TX 77030, USA. [18]Department of Biostatistics, The University of Texas MD Anderson Cancer Center, Houston, TX 77030, USA. [19]Department of Genitourinary Medical Oncology, The University of Texas MD Anderson Cancer Center, Houston, TX 77030, USA.

*These authors contributed equally to this work. †Present address: University of Rochester James P. Wilmot Cancer Center, Rochester, NY 14642, USA. ‡Present address: A.C.Camargo Cancer Center, São Paolo, Brazil. §Present address: Moffitt Cancer Center, Tampa, FL 33612, USA. ||Present address: Harvard University, Cambridge, MA 02138, USA. ¶Present address: MedImmune, Gaithersburg, MD 20878, USA. #These authors contributed equally to this work.
**Corresponding author. Email: jwargo@mdanderson.org

sequencing, noting that both communities were relatively diverse with a high abundance of bacteria of the order Lactobacillales in the oral microbiome and Bacteroidales in the fecal microbiome (Fig. 1B). Bipartite network analysis (25) demonstrated a clear separation of community structure between the oral and fecal microbiomes in terms of both matched and aggregate samples (fig. S4), suggesting that these communities are distinct in terms of their compositional structure. Loss of microbial diversity (dysbiosis) is associated with chronic health conditions (26–28) and cancer (8–10) and is also associated with poor outcomes of certain forms of cancer therapy, including allogeneic stem

cell transplant (29). Based on these data, we examined the diversity of the oral and gut microbiomes in eligible patients on anti–PD-1 therapy and found that alpha diversity, or within-sample diversity, of the gut microbiome was significantly higher in R ($n$ = 30) compared to NR ($n$ = 13) using several indices ($P$ < 0.01; Fig. 1C and fig. S5). No significant differences were observed in the oral microbiome (R = 54, NR = 32, $P$ = 0.11; fig. S6). We then tested the relationship of diversity and progression-free survival (PFS) in our cohort by stratifying patients based on tertiles of inverse Simpson scores, demonstrating that patients in the highest tertile of fecal alpha diversity had sig-

nificantly prolonged PFS compared to those with intermediate or low diversity ($P$ = 0.02 and 0.04, respectively; Fig. 1, D and E, and fig. S7). No differences in PFS were noted when comparing diversity of the oral microbiome (fig. S8). Importantly, upon visualizing beta diversity, or between-sample diversity, with weighted UniFrac distances (30) by principal coordinate analysis, we found a notable clustering effect by response status in the gut microbiome of these patients, which was not observed in the oral microbiome (Fig. 1F and fig. S8E).

Because compositional differences in the microbiome may also influence cancer development and
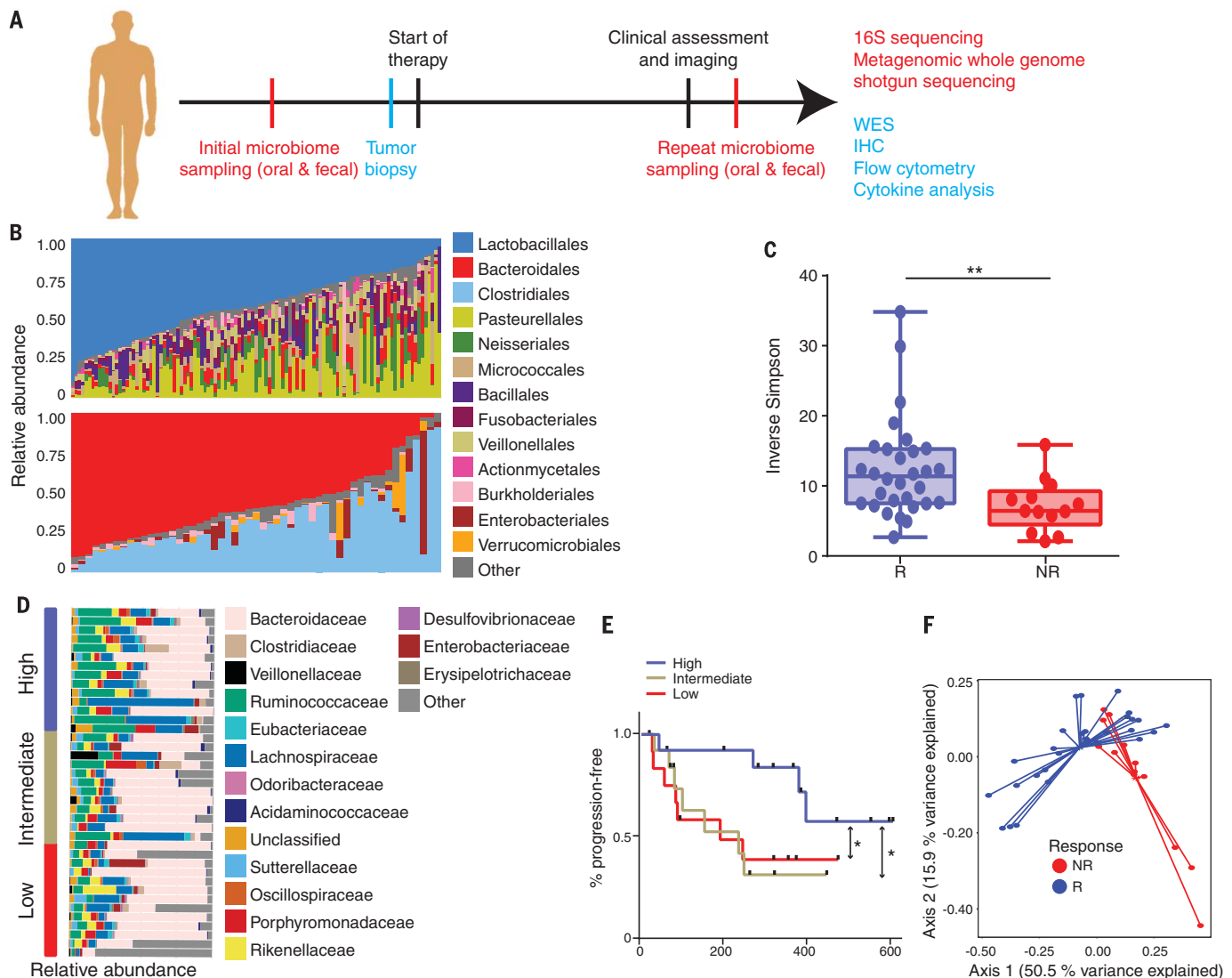


**Fig. 1. Higher gut microbiome diversity is associated with improved response to anti–PD-1 immunotherapy in patients with metastatic melanoma.** (**A**) Schema of sample collection and analyses. (**B**) Stacked bar plot of phylogenetic composition of common bacterial taxa (>0.1% abundance) at the order level in oral ($n$ = 109, top) and fecal ($n$ = 53, bottom) samples by 16S rRNA sequencing. (**C**) Inverse Simpson diversity scores of the gut microbiome in R ($n$ = 30) and NR ($n$ = 13) to anti–PD-1 immunotherapy by Mann-Whitney $U$ rank sum (MW) test. Error bars represent the distribution of diversity scores. (**D**) Phylogenetic composition of fecal samples ($n$ = 39)

at the family level (>0.1% abundance) at baseline. High [blue, >11.63 (inverse Simpson score), $n$ = 13], intermediate (gold, 7.46 to 11.63, $n$ = 13), and low (red, <7.46, $n$ = 13) diversity groups were determined using tertiles of inverse Simpson scores. (**E**) Kaplan-Meier (KM) plot of PFS by fecal diversity: high (median PFS undefined), intermediate (median PFS = 232 days), and low (median PFS = 188 days). High versus intermediate diversity (HR 3.60, 95% CI 1.02 to 12.74) and high versus low (HR 3.57, 95% CI 1.02 to 12.52) by univariate Cox model. (**F**) Principal coordinate analysis of fecal samples ($n$ = 43) by response using weighted UniFrac distances. *$P$ < 0.05; **$P$ < 0.01.
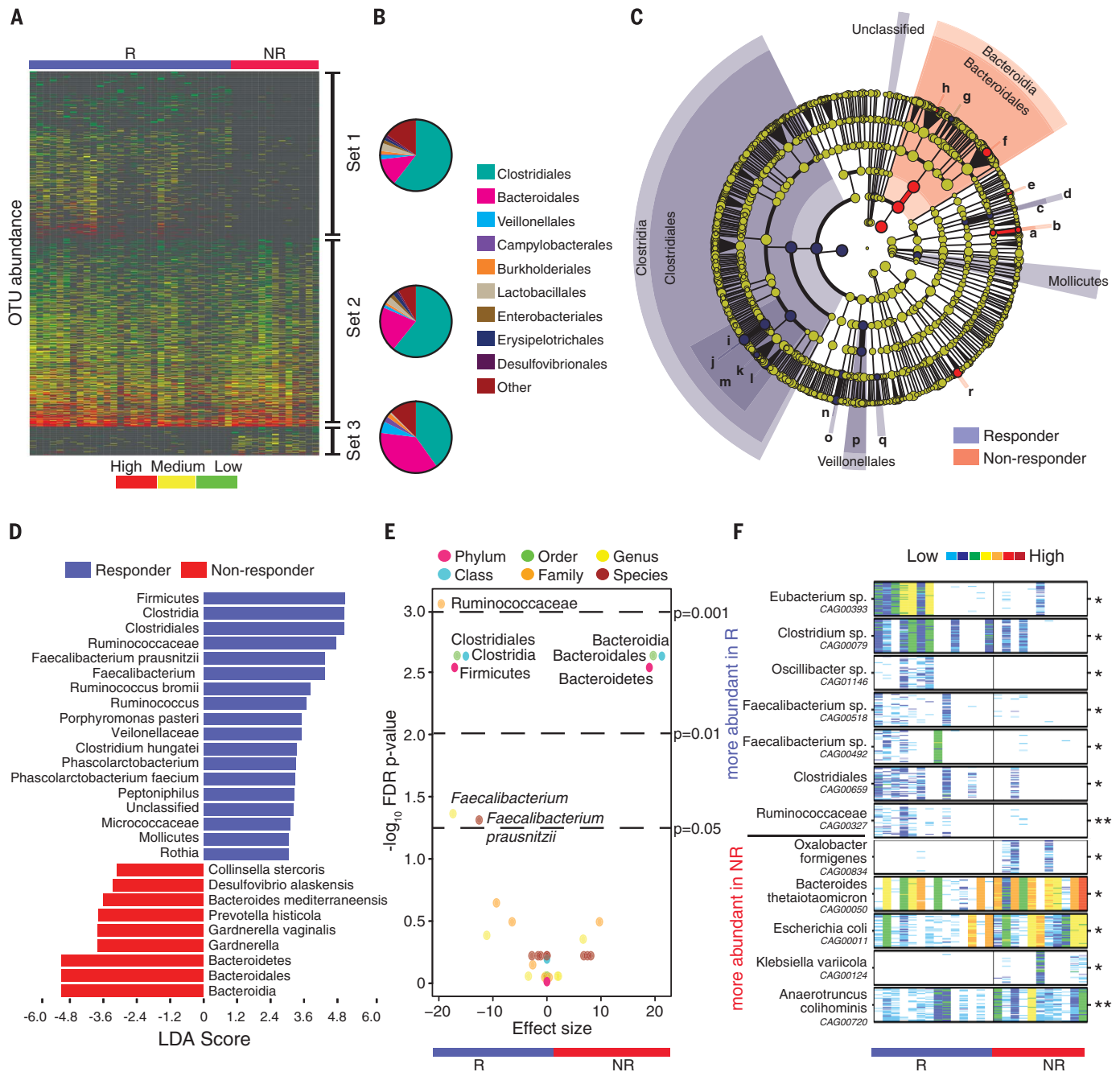
**Fig. 2. Compositional differences in the gut microbiome are associated with responses to anti−PD-1 immunotherapy.** (**A**) Heatmap of OTU abundances in R (*n* = 30) and NR (*n* = 13). Columns denote patients grouped by response and sorted by diversity within R and NR groups; rows denote bacterial OTUs grouped into three sets according to their enrichment and/or depletion in R versus NR and then sorted by mean abundance within each set. Set 1 (enriched in R), Set 2 (unenriched), and Set 3 (enriched in NR). (**B**) Phylogenetic composition of OTUs within each set described in (A) at the order level. (**C**) Taxonomic cladogram from LEfSe showing differences in fecal taxa. Dot size is proportional to the abundance of the taxon. Letters correspond to the following taxa: (a) *Gardnerella vaginalis*, (b) Gardnerella, (c) *Rothia*, (d) *Micrococcaceae*, (e) *Collinsella stercoris*, (f) *Bacteroides mediterraneensis*, (g) *Porphyromonas pasteri*, (h) *Prevotella histicola*, (i) *Faecalibacterium prausnitzii*, (j) *Faecalibacterium*, (k) *Clostridium hungatei*, (l) *Ruminococcus bromii*, (m) Ruminococcaceae, (n) *Phascolarctobacterium*

*faecium*, (o) *Phascolarctobacterium*, (p) *Veilonellaceae*, (q) *Peptoniphilus*, and (r) *Desulfovibrio alaskensis*. (**D**) Linear discriminant analysis (LDA) scores computed for differentially abundant taxa in the fecal microbiomes of R (blue) and NR (red). Length indicates effect size associated with a taxon. *P* = 0.05 for the Kruskal-Wallis *H* statistic; LDA score > 3. (**E**) Differentially abundant gut bacteria in R (blue) versus NR (red) by MW test [false-discovery rate (FDR)–adjusted] within all taxonomic levels. (**F**) Pairwise comparisons by MW test of abundances of metagenomic species identified by metagenomic WGS sequencing in fecal samples (*n* = 25) for R (*n* = 14, blue) and NR (*n* = 11, red). \**P* < 0.05; \*\**P* < 0.01. Colors reflect gene abundances visualized as "barcodes" with the following order of intensity: white (0) < light blue < blue < green < yellow < orange < red for increasing abundance, where each color change corresponds to a fourfold abundance change. In these barcodes, metagenomic species appear as vertical lines (coabundant genes in a sample) colored according to the gene abundance.

response to therapy (*12, 14, 15, 23*), we sought to determine if differences existed in the oral or gut microbiomes of R and NR to anti–PD-1 therapy. To test this, we first compared an enrichment of operational taxonomic units (OTUs) in R versus NR, demonstrating that distinct sets of rare low abundance OTUs were associated with response to anti–PD-1 therapy, with enrichment of orders Clostridiales in R and Bacteroidales in NR in the gut microbiome (*P* < 0.01; Fig. 2, A and B, and fig. S9, A and C). No significant differences in enrichment were noted in the oral microbiome

of R versus NR (fig. S9, B and D, and fig. S10). To further explore these findings, we performed high-dimensional class comparisons using linear discriminant analysis of effect size (LEfSe) (*31*), which again demonstrated differentially abundant bacteria in the fecal microbiome of R versus NR
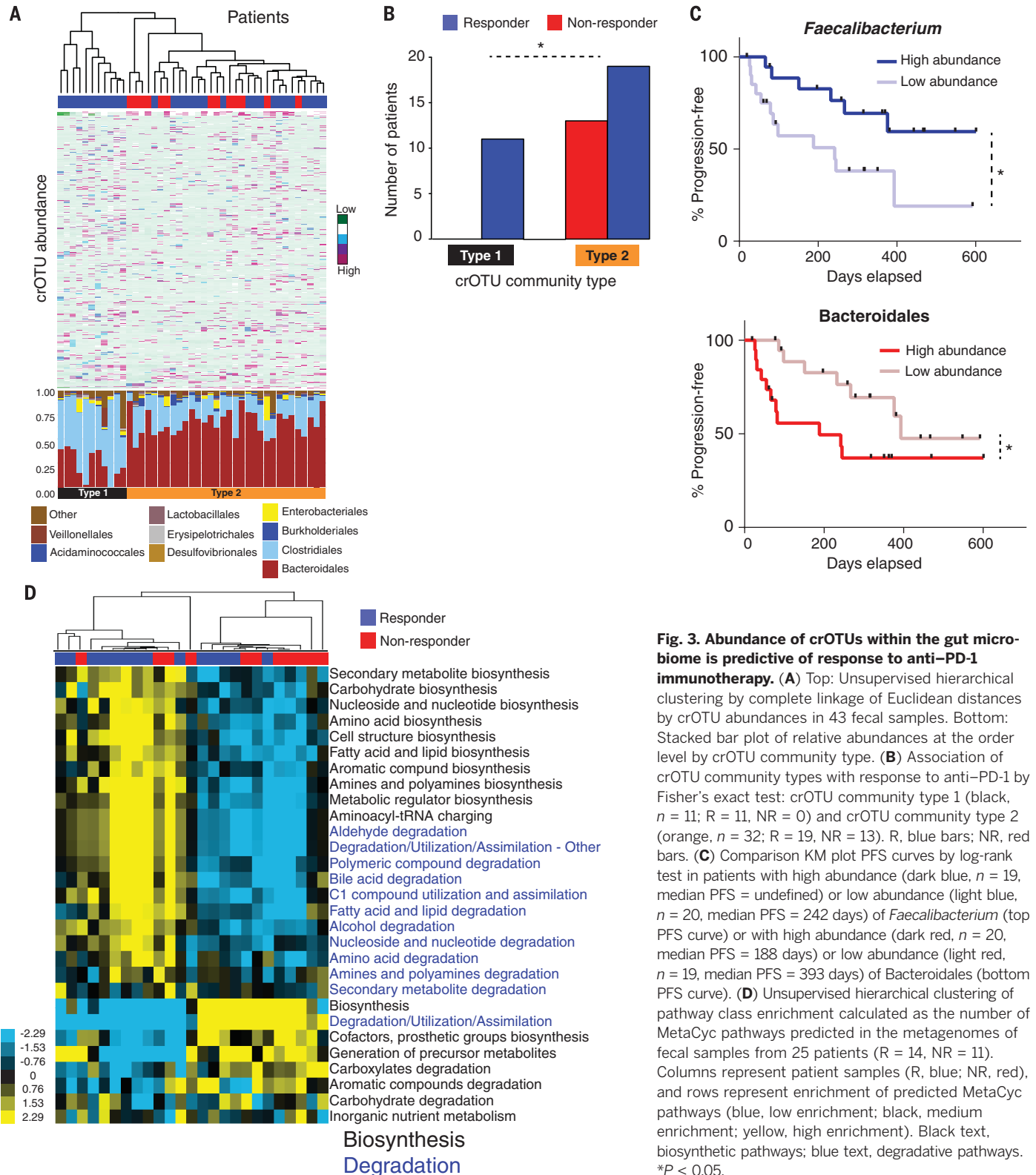


**Fig. 3. Abundance of crOTUs within the gut micro-biome is predictive of response to anti–PD-1 immunotherapy.** (**A**) Top: Unsupervised hierarchical clustering by complete linkage of Euclidean distances by crOTU abundances in 43 fecal samples. Bottom: Stacked bar plot of relative abundances at the order level by crOTU community type. (**B**) Association of crOTU community types with response to anti–PD-1 by Fisher's exact test: crOTU community type 1 (black, *n* = 11; R = 11, NR = 0) and crOTU community type 2 (orange, *n* = 32; R = 19, NR = 13). R, blue bars; NR, red bars. (**C**) Comparison KM plot PFS curves by log-rank test in patients with high abundance (dark blue, *n* = 19, median PFS = undefined) or low abundance (light blue, *n* = 20, median PFS = 242 days) of *Faecalibacterium* (top PFS curve) or with high abundance (dark red, *n* = 20, median PFS = 188 days) or low abundance (light red, *n* = 19, median PFS = 393 days) of Bacteroidales (bottom PFS curve). (**D**) Unsupervised hierarchical clustering of pathway class enrichment calculated as the number of MetaCyc pathways predicted in the metagenomes of fecal samples from 25 patients (R = 14, NR = 11). Columns represent patient samples (R, blue; NR, red), and rows represent enrichment of predicted MetaCyc pathways (blue, low enrichment; black, medium enrichment; yellow, high enrichment). Black text, biosynthetic pathways; blue text, degradative pathways. *P < 0.05.

in response to anti–PD-1 therapy, with Clostridiales order and Ruminococcaceae family enriched in R and Bacteroidales order enriched in NR (Fig. 2, C and D). No major differences were observed in the oral microbiome between R and NR, with the exception of higher Bacteroidales in NR in response to anti–PD-1 therapy (fig. S11). Pairwise comparisons were then performed for bacterial taxa at all levels by response. In addition to confirming the previous taxonomic differences, these analyses identified the *Faecalibacterium* genus as significantly enriched in R (Fig. 2E and table S3). Metagenomic WGS sequencing further confirmed enrichment of *Faecalibacterium* species in addition to others in R, whereas *Bacteroides thetaiotaomicron, Escherichia coli,* and *Anaerotruncus colihominis* were enriched in NR (Fig. 2F and table S4). Importantly, the gut microbiome was shown to be relatively stable over time in a limited number of longitudinal samples tested (fig. S12).

We next asked whether bacterial composition and abundances within the gut and/or oral microbiomes of patients were associated with a specific treatment outcome to anti–PD-1 therapy. We grouped all identified OTUs into clusters of related OTUs (crOTUs) by means of construction of a phylogenetic tree from sequence-alignment data (*32*). This technique involves comparison of abundances of different potential groupings of bacteria based on 16*S* sequence similarity and helps address the sparse distribution of OTU abundances observed in the absence of this approach (fig. S13). Unsupervised hierarchical clustering of crOTU abundances within the gut and oral microbiomes was then performed without input of response data. We found that patients segregated into two distinct community types. Type 1 was composed entirely of R and was enriched for Clostridiales, whereas type 2 comprised a mixture of R and NR (*P* = 0.02) and was enriched for Bacteroidales (Fig. 3A). To better understand compositional differences between these crOTU community types, we again performed pairwise comparisons of the gut microbiota and identified a pattern very similar to that seen when clustering by response, with Clostridiales and Ruminococcaceae enriched in type 1, and Bacteroidales enriched in type 2 (fig. S14A and table S5). Further, these communities clustered distinctly using principal coordinate analysis of weighted UniFrac distances (fig. S14B). Analysis of crOTUs in the oral microbiome revealed no apparent relationship to treatment response (fig. S15, A and B).

To explore how specific bacterial taxa affect patient treatment response, we compared PFS following anti–PD-1 therapy as it related to the "top hits" that were consistently observed across our analyses. From the Ruminococcaceae family of the Clostridiales order, we focused on the *Faecalibacterium* genus in R and Bacteroidales order in NR and stratified patients into high versus low categories on the basis of the median relative abundance of these taxa in the gut microbiome. Patients with high *Faecalibacterium* abundance had a significantly prolonged PFS versus those with a low abundance (*P* = 0.03). Conversely, pa-

tients with a high abundance of Bacteroidales had a shortened PFS compared to that of those with a low abundance (*P* = 0.05, Fig. 3D). This is in line with recently published data on CTLA-4 blockade, where patients with a higher abundance of *Faecalibacterium* had a prolonged PFS compared to those with a higher abundance of Bacteroidales in the gut microbiome (*33*). In addition, univariate Cox proportional hazards analyses demonstrated that the strongest microbial predictors of response to anti–PD-1 therapy were alpha diversity [intermediate hazard ratio (HR) = 3.60, 95% CI = 1.02 to 12.74; low HR = 3.57, 95% CI = 1.02 to 12.52] and abundance of *Faecalibacterium* (HR = 2.92, 95% CI = 1.08 to 7.89) and Bacteroidales (HR = 0.39, 95% CI = 0.15 to 1.03) in the fecal microbiome. Our final multivariate model was selected by forward stepwise selection and included *Faecalibacterium* abundance (HR = 2.95, 95% CI = 1.31 to 7.29, *P* = 0.03) and prior immunotherapy (HR = 2.87, 95% CI = 1.10 to 7.89, *P* = 0.03) (table S6). Abundance of *Faecalibacterium* and Bacteroidales also outperformed relevant clinical variables in receiver operating characteristic curve (ROC) analysis (fig. S16).

Next, we sought to gain insight into the mechanism through which the gut microbiome may influence response to anti–PD-1 therapy. We first conducted functional genomic profiling of gut microbiome samples using metagenomic WGS sequencing (*n* = 25) in R (*n* = 14) versus NR (*n* = 11). Organism-specific gene hits were assigned to the Kyoto Encyclopedia of Genes and Genomes (KEGG) orthology (KO), and, on the basis of these annotations, metagenomes for each sample were reconstructed into metabolic pathways using the MetaCyc hierarchy of pathway classifications (*34, 35*). Unsupervised hierarchical clustering of predicted pathway enrichment identified two groups of patient samples, with response rates of 69.2 and 41.7% (Fig. 3E). A similar pattern was also noted for KO abundances with 70.6 and 37.5% response rates (fig. S17). Comparisons of pathway enrichment across these groups showed differences in metabolic functions, with anabolic functions predominating in R—including amino acid biosynthesis (Fig. 3E), which may promote host immunity (*36*)—and catabolic functions predominating in NR (Fig. 3E, fig. S16, and table S7).

There is clear evidence in preclinical models that differential composition of the gut microbiome may influence therapeutic responses to anti–PD-1 therapy at the level of the tumor microenvironment (*12*); thus, we next examined the relationship between the gut microbiota and systemic and antitumor immune responses in our cohort of patients on anti–PD-1 therapy. We compared the tumor-associated immune infiltrates using multiparameter immunohistochemistry (IHC) and observed a higher density of CD8$^+$ T cells in baseline samples of R versus NR (*P* = 0.04), consistent with prior reports (Fig. 4A and fig. S18) (*18, 37*). Pairwise comparisons using Spearman rank correlations were then performed between specific bacterial taxa enriched in the

gut microbiome of R and NR and immune markers in the tumor microenvironment, demonstrating a statistically significant positive correlation between the CD8$^+$ T cell infiltrate in the tumor and abundance of the *Faecalibacterium* genus, the Ruminococcaceae family, and the Clostridiales order in the gut and a nonsignificant but negative correlation with Bacteroidales (Fig. 4, B and C, and figs. S19 and S20). No associations were seen between CD8$^+$ T cell density and diversity or crOTU community type membership (fig. S21). Analysis of systemic immune responses using flow cytometry and cytokine assays revealed that patients with a high abundance of Clostridiales, Ruminococcaceae, or *Faecalibacterium* in the gut had higher frequencies of effector CD4$^+$ and CD8$^+$ T cells in the systemic circulation with a preserved cytokine response to anti–PD-1 therapy, whereas patients with a higher abundance of Bacteroidales in the gut microbiome had higher frequencies of regulatory T cells (T$_{regs}$) and myeloid-derived suppressor cells (MDSCs) in the systemic circulation, with a blunted cytokine response (Fig. 4D and figs. S22 and S23). To better understand the influence of compositional differences in the gut microbiome on antigen processing and presentation within the tumor microenvironment, we next performed multiplex IHC targeting the myeloid compartment (*38*). In these studies, patients with a high abundance of *Faecalibacterium* in the gut microbiome had a higher density of immune cells and markers of antigen processing and presentation compared to that of patients with a high abundance of Bacteroidales (Fig. 4, E and F, and figs. S24 and S25), suggesting a possible mechanism through which the gut microbiome may modulate antitumor immune responses (*12*), though this must be validated in a larger cohort.

To investigate a causal link between a "favorable" gut microbiome and response to immune checkpoint blockade, we performed fecal microbiota transplantation (FMT) experiments in germfree recipient mice (Fig. 4G). In these studies, mice that were transplanted with stool from responders to anti–PD-1 therapy (R-FMT) had significantly reduced tumor size (*P* = 0.04; Fig. 4H and fig. S26A) by day 14 compared to those transplanted with stool from NR (NR-FMT). Importantly, mice transplanted with R-FMT stool also exhibited improved responses to anti–PD-L1 (PD-1 ligand 1) therapy (Fig. 4I) in contrast to mice that were transplanted with stool from NR (NR-FMT). Next, we performed 16S sequencing on fecal samples collected from mice treated with FMT, demonstrating that mice transplanted with R-FMT stool also had significantly higher abundance of *Faecalibacterium* in their gut microbiome (*P* < 0.01) (fig. S27). We also wanted to better understand the mechanism through which the gut microbiome may influence systemic and antitumor immune responses, and so we performed correlative studies on tumors, peripheral blood, and spleens from these mice. These studies demonstrated that tumors of mice receiving R-FMT stool had a higher density of CD8$^+$ T cells than mice receiving NR-FMT, consistent
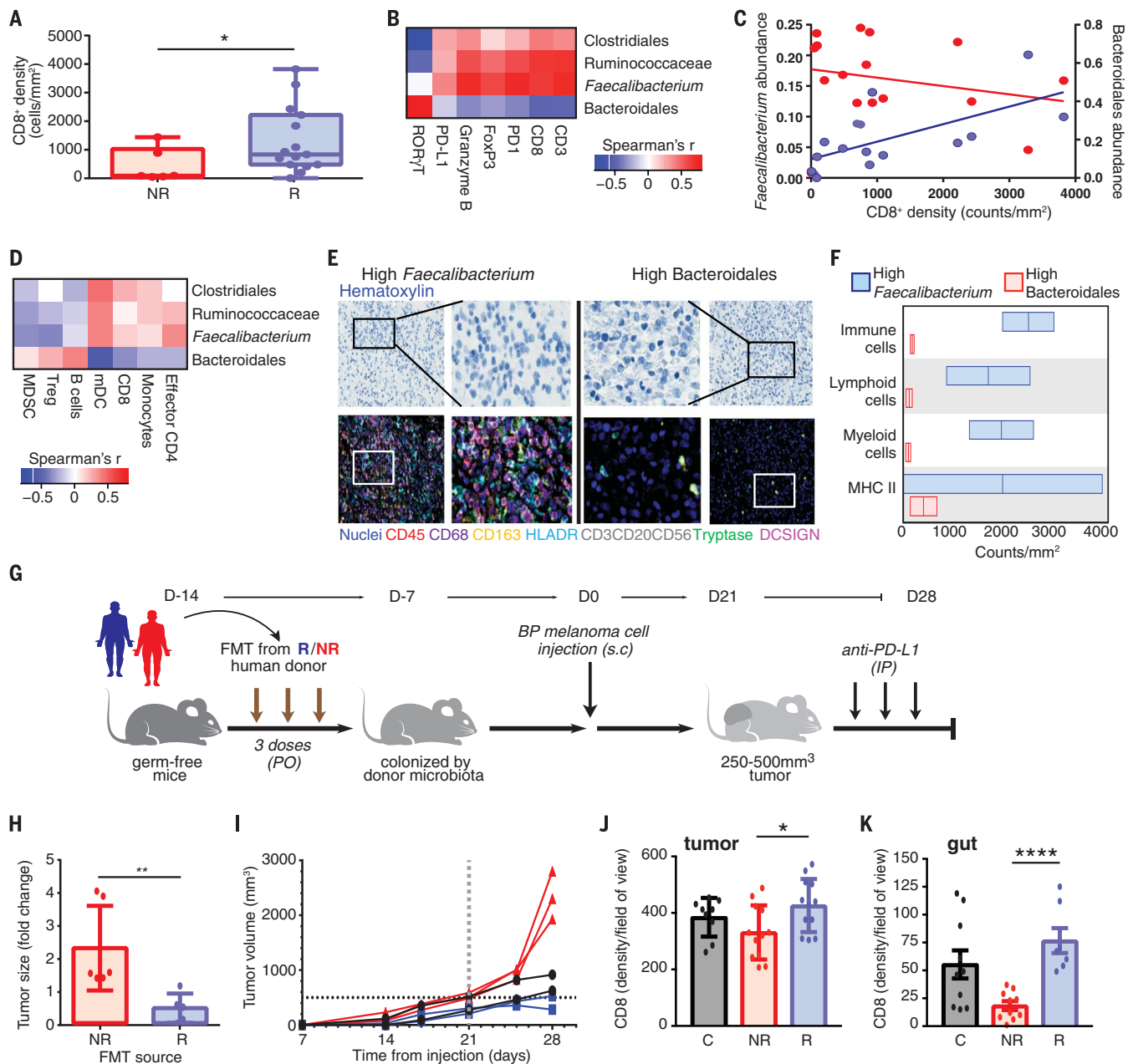
**Fig. 4. A favorable gut microbiome is associated with enhanced systemic and antitumor immunity.** (**A**) Quantification by IHC of the CD8+ T cell infiltrate at pretreatment in tumors in R (*n* = 15, blue) and NR (*n* = 6, red) by one-sided MW test. Error bars represent the distribution of CD8+ T cell densities. (**B**) Pairwise Spearman rank correlation heatmap of significantly different taxa in fecal samples (*n* = 15) at baseline and CD3, CD8, PD-1, FoxP3, Granzyme B, PD-L1, and RORγT density in matched tumors. (**C**) Univariate linear regression between CD8+ T cell density in counts per mm$^2$ in the tumor versus *Faecalibacterium* [blue, coefficient of determination ($R^2$) = 0.42, *P* < 0.01] and Bacteroidales (red, $R^2$ = 0.06, *P* = 0.38) abundance in the gut. (**D**) Pairwise Spearman rank correlation heatmap between significantly different fecal taxa and frequency of indicated cell types by flow cytometry in peripheral blood at baseline. mDC, myeloid dendritic cell. (**E**) Representative multiplex IHC images and (**F**) frequency of various immune cell types in patients having high *Faecalibacterium* (*n* = 2) or Bacteroidales (*n* = 2) in the gut. In (E), rectangles identify magnified region. MHC II, major histocompatibility complex II. (**G**) Experimental design of studies in germ-free (GF) mice. Time in days (indicated as D) relative to tumor injection (2.5 × 10$^5$ to 8 × 10$^5$ tumor cells). PO, per os (orally); BP, *BRAF*$^{V600E}$/*PTEN*$^{-/-}$; s.c., subcutaneous;

IP, intraperitoneal. (**H**) Difference in size by MW test of tumors at day 14, implanted in R-FMT (blue) and NR-FMT mice (red), expressed as fold change (FC) relative to average tumor volume of control GF mice. Data from two independent FMT experiments (R-FMT, *n* = 5, median FC = 0.18; NR-FMT, *n* = 6, median FC = 1.52). (**I**) Representative tumor growth curves for each GF mouse from anti–PD-L1 treated R-FMT (blue, *n* = 2, median tumor volume = 403.7 mm$^3$), NR-FMT (red, *n* = 3, median tumor volume = 2301 mm$^3$), and control (black, *n* = 2, median tumor volume = 771.35 mm$^3$) mice. Statistics are as follows: *P* = 0.20 (R-FMT versus NR-FMT) and *P* = 0.33 (NR-FMT versus control) by MW test. Dotted black line marks tumor-size cutoff for anti–PD-L1 treatment (500mm$^3$). (**J**) Quantification of CD8+ density in tumor of R-FMT [*n* = 2, median = 433.5 cells/high-power field (HPF) across 12 regions], NR-FMT (*n* = 2, median = 325 cells/HPF across 12 regions), and control mice (*n* = 2, median = 412 cells/HPF across 9 regions). MW test *P* = 0.30 (R-FMT versus control). (**K**) Quantification of CD8+ density in gut R-FMT (*n* = 2, median = 67 cells/HPF across 7 regions), NR-FMT (*n* = 2, median = 24 cells/HPF across 5 regions), and control (*n* = 2, median = 47 cells/HPF across 10 regions). MW test *P* = 0.17 (R-FMT versus control). *P* < 0.05; **P* < 0.01; ****P* < 0.0001.

with human data (Fig. 4J and fig. S26B, top series). Analysis of CD45$^+$ myeloid and lymphoid tumor-infiltrating cells by flow cytometry confirmed this result (fig. S26C). Moreover, FMT from R locally increased the number of CD45$^+$ immune and CD8$^+$ T cells in the gut compared to FMT from NR (Fig. 4K and fig. S26B, bottom series). Mass cytometry analysis using t-distributed stochastic neighbor embedding dimension reduction was performed on tumors from mice and demonstrated up-regulation of PD-L1 in the tumor microenvironment of mice receiving R-FMT versus NR-FMT stool (fig. S26D), suggesting the development of a "hot" tumor microenvironment. Further phenotypic studies of tumor immune infiltrates revealed a significant enrichment of innate effector cells (expressing CD45$^+$CD11b$^+$Ly6G$^+$) in mice receiving R-FMT stool (fig. S26E). A lower frequency of suppressive myeloid cells (expressing CD11b$^+$CD11c$^+$) was observed in mice receiving R-FMT stool compared to that of mice receiving NR-FMT (fig. S26F). Finally, an increase in the frequency of RORγT$^+$ T helper 17 cells in the tumor was also detected in mice transplanted with NR-FMT stool (fig. S26G), in line with what we observed in tumors from patients who failed to respond to anti–PD-1 therapy. Mice receiving NR-FMT stool also had higher frequencies of regulatory CD4$^+$FoxP3$^+$ T cells (fig. S26H) and CD4$^+$IL-17$^+$ T cells (fig. S26I) in the spleen, suggesting impaired host immune responses.

Our results indicate that the gut microbiome may modulate responses to anti–PD-1 immunotherapy in melanoma patients. We propose that patients with a favorable gut microbiome (for example, high diversity and abundance of Ruminococcaceae and *Faecalibacterium*) have enhanced systemic and antitumor immune responses mediated by increased antigen presentation and improved effector T cell function in the periphery and the tumor microenvironment. By contrast, patients with an unfavorable gut microbiome (for example, low diversity and high relative abundance of Bacteroidales) have impaired systemic and antitumor immune responses mediated by limited intratumoral lymphoid and myeloid infiltration and weakened antigen presentation capacity. These findings highlight the therapeutic potential of modulating the gut microbiome in patients receiving checkpoint blockade immunotherapy and warrant prompt evaluation in cancer patients through clinical trials.

## REFERENCES AND NOTES

1. D. Schadendorf et al., *J. Clin. Oncol.* **33**, 1889–1894 (2015).
2. C. Robert et al., *N. Engl. J. Med.* **372**, 2521–2532 (2015).
3. C. Robert et al., *N. Engl. J. Med.* **372**, 320–330 (2015).
4. M. D. Vesely, R. D. Schreiber, *Ann. N. Y. Acad. Sci.* **1284**, 1–5 (2013).
5. S. L. Topalian, C. G. Drake, D. M. Pardoll, *Cancer Cell* **27**, 450–461 (2015).
6. E. Tran, P. F. Robbins, S. A. Rosenberg, *Nat. Immunol.* **18**, 255–262 (2017).
7. P. Bachireddy, U. E. Burkhardt, M. Rajasagi, C. J. Wu, *Nat. Rev. Cancer* **15**, 201–215 (2015).
8. W. S. Garrett, *Science* **348**, 80–86 (2015).
9. J. A. Segre, *Science* **349**, 1058–1059 (2015).
10. J. L. Drewes, F. Housseau, C. L. Sears, *Br. J. Cancer* **115**, 273–280 (2016).
11. C. M. Paulos et al., *J. Clin. Invest.* **117**, 2197–2204 (2007).
12. A. Sivan et al., *Science* **350**, 1084–1089 (2015).
13. N. Iida et al., *Science* **342**, 967–970 (2013).
14. S. Viaud et al., *Science* **342**, 971–976 (2013).
15. L. H. Schwartz et al., *Eur. J. Cancer* **62**, 132–137 (2016).
16. A. Snyder et al., *N. Engl. J. Med.* **371**, 2189–2199 (2014).
17. P. Sharma et al., *Lancet Oncol.* **18**, 312–322 (2017).
18. P. L. Chen et al., *Cancer Discov.* **6**, 827–837 (2016).
19. W. Roh et al., *Sci. Transl. Med.* **9**, eaah3560 (2017).
20. E. M. Van Allen et al., *Science* **350**, 207–211 (2015).
21. N. McGranahan et al., *Science* **351**, 1463–1469 (2016).
22. W. Hugo et al., *Cell* **165**, 35–44 (2016).
23. D. B. Johnson et al., *Cancer Immunol. Res.* **4**, 959–967 (2016).
24. N. A. Rizvi et al., *Science* **348**, 124–128 (2015).
25. B. D. Muegge et al., *Science* **332**, 970–974 (2011).
26. Human Microbiome Project Consortium, *Nature* **486**, 207–214 (2012).
27. P. J. Turnbaugh, F. Bäckhed, L. Fulton, J. I. Gordon, *Cell Host Microbe* **3**, 213–223 (2008).
28. J. Qin et al., *Nature* **464**, 59–65 (2010).
29. Y. Taur et al., *Blood* **124**, 1174–1182 (2014).
30. C. Lozupone, M. E. Lladser, D. Knights, J. Stombaugh, R. Knight, *ISME J.* **5**, 169–172 (2011).
31. N. Segata et al., *Genome Biol.* **12**, R60 (2011).
32. J. U. Peled et al., *J. Clin. Oncol.* **35**, 1650–1659 (2017).
33. N. Chaput et al., *Ann. Oncol.* **28**, 1368–1379 (2017).
34. R. Caspi et al., *Nucleic Acids Res.* **36**, D623–D631 (2008).
35. M. Kanehisa, S. Goto, *Nucleic Acids Res.* **28**, 27–30 (2000).
36. E. Blacher, M. Levy, E. Tatirovsky, E. Elinav, *J. Immunol.* **198**, 572–580 (2017).
37. P. C. Tumeh et al., *Nature* **515**, 568–571 (2014).
38. T. Tsujikawa et al., *Cell Reports* **19**, 203–217 (2017).

# Science

## Gut microbiome modulates response to anti–PD-1 immunotherapy in melanoma patients

V. Gopalakrishnan, C. N. Spencer, L. Nezi, A. Reuben, M. C. Andrews, T. V. Karpinets, P. A. Prieto, D. Vicente, K. Hoffman, S. C. Wei, A. P. Cogdill, L. Zhao, C. W. Hudgens, D. S. Hutchinson, T. Manzo, M. Petaccia de Macedo, T. Cotechini, T. Kumar, W. S. Chen, S. M. Reddy, R. Szczepaniak Sloane, J. Galloway-Pena, H. Jiang, P. L. Chen, E. J. Shpall, K. Rezvani, A. M. Alousi, R. F. Chemaly, S. Shelburne, L. M. Vence, P. C. Okhuysen, V. B. Jensen, A. G. Swennes, F. McAllister, E. Marcelo Riquelme Sanchez, Y. Zhang, E. Le Chatelier, L. Zitvogel, N. Pons, J. L. Austin-Breneman, L. E. Haydu, E. M. Burton, J. M. Gardner, E. Sirmans, J. Hu, A. J. Lazar, T. Tsujikawa, A. Diab, H. Tawbi, I. C. Glitza, W. J. Hwu, S. P. Patel, S. E. Woodman, R. N. Amaria, M. A. Davies, J. E. Gershenwald, P. Hwu, J. E. Lee, J. Zhang, L. M. Coussens, Z. A. Cooper, P. A. Futreal, C. R. Daniel, N. J. Ajami, J. F. Petrosino, M. T. Tetzlaff, P. Sharma, J. P. Allison, R. R. Jenq and J. A. Wargo

### Good bacteria help fight cancer

Resident gut bacteria can affect patient responses to cancer immunotherapy (see the Perspective by Jobin). Routy *et al.* show that antibiotic consumption is associated with poor response to immunotherapeutic PD-1 blockade. They profiled samples from patients with lung and kidney cancers and found that nonresponding patients had low levels of the bacterium *Akkermansia muciniphila*. Oral supplementation of the bacteria to antibiotic-treated mice restored the response to immunotherapy. Matson *et al.* and Gopalakrishnan *et al.* studied melanoma patients receiving PD-1 blockade and found a greater abundance of "good" bacteria in the guts of responding patients. Nonresponders had an imbalance in gut flora composition, which correlated with impaired immune cell activity. Thus, maintaining healthy gut flora could help patients combat cancer.

*Science*, this issue p. 91, p. 104, p. 97; see also p. 32

| | |
|---|---|
| **ARTICLE TOOLS** | http://science.sciencemag.org/content/359/6371/97 |
| **SUPPLEMENTARY MATERIALS** | http://science.sciencemag.org/content/suppl/2017/11/01/science.aan4236.DC1 |
| **RELATED CONTENT** | http://science.sciencemag.org/content/sci/359/6371/91.full<br>http://science.sciencemag.org/content/sci/358/6363/573.full<br>http://science.sciencemag.org/content/sci/359/6371/32.full<br>http://science.sciencemag.org/content/sci/359/6371/104.full<br>http://stm.sciencemag.org/content/scitransmed/8/328/328rv4.full<br>http://stm.sciencemag.org/content/scitransmed/7/271/271ps1.full |
| **REFERENCES** | This article cites 76 articles, 20 of which you can access for free<br>http://science.sciencemag.org/content/359/6371/97#BIBL |

Use of this article is subject to the Terms of Service